Available online at www.sciencedirect.com
SCIENCE DIRECT
Diamond & Related Materials 15 (2006) 898 – 903
DIAMOND AND RELATED MATERIALS
www.elsevier.com/locate/diamond

Roughness evolution during growth of hydrogenated tetrahedral amorphous carbon

S. Pisana *, C. Casiraghi, A.C. Ferrari, J. Robertson

Department of Engineering, University of Cambridge, Cambridge CB2 1PZ, UK

Available online 11 January 2006

Abstract

Hydrogenated tetrahedral amorphous carbon (ta-C:H) is advantageous as coating material for high-density magnetic and optical storage devices, due to its favorable combination of density and smoothness. An advantage of ta-C:H over tetrahedral amorphous carbon (ta-C) is the absence of macroparticles, often found in cathodic arc deposition of ta-C, and the hydrogen rich surface, compatible with the lubricant. As for ta-C, in order to increase the magnetic storage density, the ta-C:H thickness needs to be decreased. It is thus necessary to determine the minimum thickness for continuous and pin-hole free films. Here we investigate the roughness evolution of ta-C:H by atomic force microscopy and determine the roughness and growth exponents α and β. We find a very similar behaviour to ta-C, with the ta-C:H roughness slightly higher than the ta-C one for any given thickness. This confirms the smoothing effect of impinging ions during ta-C:H deposition.
© 2005 Elsevier B.V. All rights reserved.

Keywords: Tetrahedral amorphous carbon; Plasma CVD; Surface characterization; Surface structure

1. Introduction

Diamond-like Carbon (DLC) is an amorphous carbon with a significant fraction of C–C sp^3 bonds [1]. Tetrahedral amorphous carbon (ta-C) is the DLC with the maximum sp^3 content. Hydrogenated tetrahedral amorphous carbon (ta-C:H) is a hydrogenated amorphous carbon with the largest fraction of C–C sp^3 bonds. Indeed, due to the highest sp^3 content (~70%) and hydrogen content of 25–30 at.%, ta-C:Hs are really a different category as indicated by their Raman spectra [2,3], their higher density (up to 2.4 g/cm^3) [4] and Young's Modulus (up to 300 GPa) [5]. Their optical gap can reach 2.4 eV [6]. These films are deposited by high-density plasma sources such as Electron Cyclotron Wave Resonance (ECWR) [6–8] and Plasma Beam Source (PBS) [9,10]. Ta-C:H was also produced by introducing H while depositing ta-C by Filtered Cathodic Vacuum Arc (FCVA) [11].

The surface roughness of DLC is a key property for some of its applications. For instance, in micro-electro-mechanical systems it is desirable to keep the surface roughness at a certain level to minimize stiction [12]. The evolution of surface roughness with thickness is also crucial for the application of DLC as a protective overcoat for high density magnetic and optical storage devices [13–17].

Over the years, the need for increasing mass storage in computer systems has pushed the magnetic disk storage density to increasingly higher levels [18,19]. As the magnetic storage density increases, the distance between the read/write head and the spinning surface of the disks decreases [13,18]. In such conditions, any particulates would damage the read/write head or the surface of the disk. Furthermore, the surfaces of the disk and the read/write heads require an overcoat to protect them from contaminants, corrosion, mechanical wear and occasional contact between the disk surface and the read/write head. Therefore the protective coating should be hard, smooth, continuous and chemically inert.

Magnetron sputtered nitrogenated amorphous carbon (a-C:N) and a-C:H have been used so far as protective coatings. Ta-C has been identified as the material of choice to reach the ultimate storage density of ~1 Tbit/in.^{2} in next generation magnetic storage recording, due to its ultra-smoothness, combined with good mechanical properties and density down to nm thickness [14,20]. The major hindrance for the use of ta-C is the possible presence of macroparticles on the sample surface, which is quite challenging to avoid in a filtered cathodic arc deposition system [21,22]. Ta-C:H is potentially

* Corresponding author. Tel.: +44 1223 765242; fax: +44 1223 332662.
E-mail address: sp406@eng.cam.ac.uk (S. Pisana).

0925-9635/$ - see front matter © 2005 Elsevier B.V. All rights reserved.
doi:10.1016/j.diamond.2005.10.052

a better material than ta-C as a hard disk protective coating. It has similar roughness [6] and tribological properties to ta-C [8]. Being deposited by a plasma deposition process from a gas precursor [6–10,16], it can be used to coat large areas, such as the hard disk surface, without particulates. Also, its hydrogen-rich surface can allow a better interaction with the lubricant [18]. The lower density of ta-C:H with respect to ta-C may however raise the film thickness needed to provide corrosion protection, as is the case for magnetron sputtered a-C:N [23].

The evolution of the surface roughness of ta-C:H has not been well characterized so far. Peng et al. [24] reported a root mean square (rms) roughness of ~0.11 nm in a-C:H deposited by RF plasma enhanced chemical vapor deposition (PECVD). Weiler et al. [9] reported the average roughness of ta-C:H prepared by PBS as being less than 0.5 nm, while Sattel et al. [25] reported an average roughness of about 2 nm, when using the same system. Morrison et al. [8] reported the rms roughness of samples deposited by ECWR as being less than 0.3 nm. No systematic study of the surface evolution during growth has been reported so far.

The characterization of the evolution of a surface can be used to understand the growth process. We found that the surface roughness of ta-C remains approximately constant with thicknesses and this has been associated to the presence of surface diffusion and relaxation, due to downhill currents induced by the impinging carbon ions [14,15,17].

In this paper we extend our previous work on ta-C with a similar study on ta-C:H.

2. Experimental

The ta-C:H samples were deposited with an ECWR diffusion pumped system (CCR DN320) [6,8,10]. The depositions were carried out using C_2H_2 at a pressure of $\sim 3\times10^{-4}$ mbar, 13 Gauss magnetic field and power of 350 W at 13.56 MHz. The plasma thus obtained had a high density [1,7], an ion energy of 170 eV per ion with an energy distribution width of 20 eV at full-width half-maximum, as measured by Faraday cup. If we assume that the majority of the impinging ions are $C_2H_2^+$ [1] we can estimate an ion energy of 78 eV per carbon atom. The samples were deposited on (100) polished Si substrates (Compart Technology Sb doped, 0.015–0.025 Ω cm) cleaned in an ultrasonic bath with acetone, isopropanol and methanol.

The thickness was measured by variable angle monochrome ellipsometry (Gaertner Scientific L117), spectroscopic ellipsometry (J.A. Woolam M2000V) and atomic force microscopy (AFM). The thickness measured with the various techniques is accurate within 0.3 nm. The samples we analyze here have thickness ranging from 1 nm to 110 nm.

The optical properties were measured with a Unicam UV/Vis spectrometer. The optical gap (E_{04}) was identified at the photon energy where the optical absorption coefficient (α_{ph}) reaches a value of 10^4 cm^{-1}. The Tauc optical gap was obtained by extrapolating the linear trend exhibited by $\sqrt{\alpha_{ph}E_{ph}}$, for photon energies, E_{ph}, between 2.5 and 4 eV.

Raman spectroscopy was performed at 514 nm excitation using a Renishaw micro-Raman 1000 spectrometer. The spectra were collected using a 100× objective and the laser power was kept below 0.5 mW. The D and G band region of the spectra was fit using two Gaussian lines and the following fit parameters are considered: the Raman shift of the G peak (Pos(G)), the G peak full width at half maximum (FWHM(G)), and the ratios of the intensity and areas of the D and G peaks (I(D)/I(G) and A(D)/A(G), respectively). For the thinnest films the third order Raman peak of the silicon substrate at ~1430 cm^{-1} was removed from the D and G spectral region before fitting, as in Ref. [26].

AFM characterization was carried out with a Veeco Explorer Scanning Probe Microscope in tapping mode. The etched silicon cantilevers used were 110–140 μm long and oscillated at a frequency between 230 and 410 kHz. The cantilever tip had a radius of curvature <10 nm and was routinely replaced in order to avoid influencing the resulting topographies by tip wear. All scans were performed on an area of 1×1 μm^2 with 300 lines of resolution and were flattened to subtract the contribution of sample tilt. The data analysis was performed on 500×500 nm^2 areas within each scan and the results were averaged, to better compare with previous studies [14].

Note that for our previous work on ta-C we used a different AFM (Digital Instruments Nanoscope III) [14]. In order to directly compare the data we measure here on ta-C:H with our previous ta-C measurements, we re-measured a set of ta-C films of increasing thickness with the present Veeco Explorer AFM. We noted a systematic shift of 0.025 nm in the roughness measured, and this shift was then used to adjust our measured ta-C:H roughness accordingly.

The rms roughness is defined as follows:

$$R=\sqrt{\frac{1}{N}\sum_n (h_n-h_{ave})^2} \quad (1)$$

where N is the total number of data points, h_n is the height of the nth data point and h_{ave} is the average height of the surface. This will be referred to simply as roughness. The cleaned silicon substrates were measured to have a roughness of 0.135 nm. In Ref. [14] the silicon roughness was measured to be ~0.18 nm. This difference is due to the different silicon substrates.

3. Surface analysis

3.1. Dynamic scaling

Dynamic scaling is a powerful way of examining a surface, capable of predicting surface properties over various length scales and of correlating processes that may appear different in nature [27]. It can be used to predict the surface properties since the growth process determines how the surface grows. The scaling laws allow for the identification of different universality classes that allow for the complete characterization of complex surface with simple relations.

A first possible approach is to use the Family-Vicsek scaling relation to examine the dynamics of roughening [27,28]:

$$R(L,t) \sim L^{\alpha} f\left(\frac{t}{L^{\alpha/\beta}}\right). \quad (2)$$

Here L is the lateral size of the system, t is time (equivalent to thickness for constant deposition rates), α is called the roughness exponent, β is the growth exponent [27]. The scaling function $f(u)$ (where $u=t/t_x$) varies depending on t_x, called saturation time [27]. This is based on the assumption that as the deposition takes place and material is added to a flat substrate, the roughness will increase until, passed the saturation time, the roughness saturates and remains constant [27]. So for small thickness, where $t \ll t_x$, $f(u)=u^{\beta}$, and

$$R \sim t^{\beta}. \quad (3)$$

For large thickness, $f(u)$ is constant, and

$$R \sim L^{\alpha}. \quad (4)$$

The exponents α and β assume specific values depending on the growth mechanism. The most common growth mechanisms are: random deposition (α undefined, $\beta=0.5$) [27], random deposition with surface relaxation described by the Edwards-Wilkinson equation ($\alpha=0$, $\beta=0$) [29], nonlinear theory described by the Kardar-Parisi-Zhang equation ($\alpha \sim 0.38$, $\beta \sim 0.24$) [30], and molecular beam epitaxy ($\alpha=1$, $\beta=0.25$) [27].

Dimensional analysis is used to obtain the exponents α and β experimentally [27]. α is usually obtained by analyzing the roughness at different length scales of samples thick enough for the roughness to be saturated (Eq. (4)). Similarly, β is obtained by analyzing the roughness at different thicknesses for samples with unsaturated roughness (Eq. (3)). In DLC it can be difficult to measure α by dimensional analysis, as the thickness needs to be high enough to saturate the roughness ($t \gg t_x$) [27,31], but generally the films are at most ~100–150 nm thick.

If we assume that $\alpha \neq 0$, we can obtain α by analyzing the surface using the height–height correlation function

$$H(r) = \langle [h(r) - h(0)]^2 \rangle_r \quad (5)$$

where r is the surface position, and the brackets indicate spatial averaging for all r. The height–height correlation function can be written in terms of the scaling parameters as [27,32]:

$$H(r) = 2R^2 f\left(\frac{r}{\xi}\right), \quad (6)$$

where ξ is the correlation length. At the beginning of the growth, all surface sites are uncorrelated, and as the film grows, the surface sites may evolve both in height and in width. The correlation length is the distance within which the surface sites are correlated. $f(r/\xi)$ is a function that asymptotically tends to $(r/\xi)^{2\alpha}$ for $r<\xi$ and to 1 for $r>\xi$ [32]. Therefore in a log–log plot of the height–height correlation function, the slope of the linear part for small r is equal to 2α, while for large r it saturates to $2R^2$. Then another way to obtain β, known α, is through the kinetics of ξ, since [27]

$$\xi \sim t^{\beta/\alpha}. \quad (7)$$

However, if the surface evolution is described by the Edwards-Wilkinson model, then $\alpha=0$ and $\beta=0$. Yet the scaling law $z=\alpha/\beta$ remains defined, with $z=2$, and R scales with L [27]. In this case then, the height–height correlation function cannot be used to estimate α and β, and frequency analysis should be used instead [27,33].

3.2. Frequency analysis

Frequency analysis consists in taking the Fourier transform of the surface topography to obtain the power spectral density (PSD). In this representation, dynamic scaling takes the form [33]:

$$\langle |h(\mathbf{k},t)|^2 \rangle = \Omega \frac{1-\exp(-2c_i|k|^i t)}{c_i|k|^i}, \quad (8)$$

where h is the surface height, t is the film thickness, c_i is a constant which depends on the lateral transport mechanism identified by i and Ω is proportional to the incoming flux. The Fourier index $i=2(\alpha+1)$ is extracted by taking the modulus of the slope of the linear region in the log–log plot of the PSD in the large wave-vector region [32,33]. In the case of the Edwards-Wilkinson model, $\alpha=0$, thus $i=2$.

4. Results and discussion

Raman spectroscopy measured at 514 nm confirmed that the ta-C:H films obtained were of good quality. Fig. 1a compares the Raman spectra for samples of 3, 13, 52 and 110 nm in thickness. Fig. 1b shows how the thinner films have a lower Pos(G) and lower FWHM(G), indicating lower densities. This can be explained in view of the loss of the denser sp^3-rich film bulk [1,2,4]. This trend closely resembles that found for ta-C films of decreasing thickness, and it can be described by the same equation [13]:

$$\mathrm{FWHM(G)}(t) = \mathrm{FWHM(G)}_{\mathrm{BULK}} - \left[\mathrm{FWHM(G)}_{\mathrm{BULK}} - \mathrm{FWHM(G)}_{\mathrm{CSi}}\right] \times t_{\mathrm{CSi}}/t, \quad (9)$$

where $\mathrm{FWHM(G)}_{\mathrm{BULK}}$ is the FWHM(G) of the bulk phase, $\mathrm{FWHM(G)}_{\mathrm{Csi}}$ is the corresponding FWHM(G) for the carbon-Si interface layer and t_{CSi} is the thickness of the interface layer. If we take FWHM(G) as the value of the thickest film and $\mathrm{FWHM(G)}_{\mathrm{Csi}}$ as that of our thinnest film, Eq. (9) describes well the structural evolution of our films as a function of thickness (Fig. 1b). A similar trend is seen for Pos(G) (Fig. 1b).

For a 19 nm thick film we get FWHM(G) ~ 195 cm^{-1}, Pos(G) ~ 1548 cm^{-1}, I(D)/I(G) ~ 0.34 and A(D)/A(G) ~ 0.42. This confirms these films are indeed ta-C:H [2,3,8]. By using the trends of Ref. [3] to estimate density and hydrogen content from the visible Raman spectra, we get density ~ 2.1 g/cm^3 and H content ~ 30 at.% for this film. The optical gap (E_{04}) and the Tauc gap (E_{T}) were directly measured to be 2.48 eV and 1.92 eV, respectively.

Fig. 2 shows the surface topography as function of film thickness. It can be seen that the roughness mildly decreases

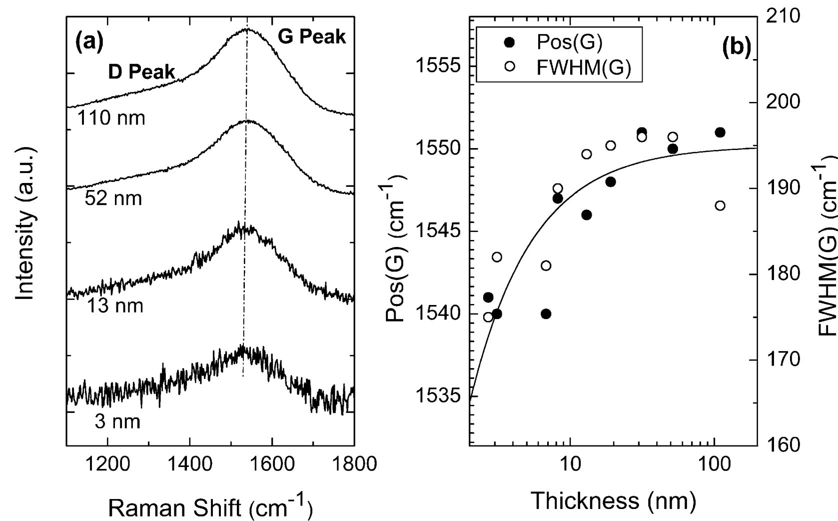

Fig. 1. (a) Raman spectra of 110 nm, 52 nm, 13 nm and 3 nm thick ta-C:H films. (b) FWHM(G) and Pos(G) as a function of film thickness. The line plots Eq. (9).

and the features on the topography become larger. Also, the topography of the thinnest films resembles the topography of the bare Si substrate. The ta-C:H films appear to be continuous for all the thicknesses analyzed. Indeed, the minimum thickness of the 1 nm film within the topographic scans is measured to be 0.8 nm, so the film seems continuous, although this is subject to the limited scan area of 1 μm^2 and the limited sharpness of the AFM tip.

Fig. 3a shows the roughness as function of film thickness. The thinner films have a roughness of 0.13 nm, close to that of the bare Si substrates. This is similar to what we previously observed for ta-C [14]. When the film thickness is larger 2–3 nm, there is a sharp decrease in roughness up to a thickness of 10–20 nm, after which the roughness remains constant at 0.11 nm. Thus, neglecting the substrate smoothening, we get a $\beta \approx 0$, as for ta-C [14,15]. Fig. 3b compares the trends of roughness as a function of film thickness we measured for ta-C with those measured here for ta-C:H. The agreement is evident, showing the universality of the underlying smoothening mechanism [15].

Under the assumption that $\alpha \neq 0$, to obtain estimates of α and β, the height–height correlation function can be used. Fig. 4 shows the height–height correlation function of some of the films analyzed. Only the films thicker than 10 nm were analyzed to exclude effects of the substrate. The slope of the data for small radial distance, where $r < \xi$, is used to find α, as previously described [14]. The saturation value for $r \gg \xi$ is related to the roughness of the films (Eq. (6)) and it corresponds to the roughness previously presented in Fig. 3. To obtain the correlation length, the height–height correlation function was fitted to the exponential [34]:

$$H(r) = 2R^2\left(1 - \exp\left(-(r/\xi)^{2\alpha}\right)\right). \quad (10)$$

The different values for α obtained are independent of the film thicknesses, with a small spread in the different values obtained, giving $\alpha = 0.32 \pm 0.05$ on average. Fig. 5 shows a log–log plot of the correlation length versus film thickness. A good trend with small spread is evident, and from here we get $\beta/\alpha = 0.29 \pm 0.07$. In conjunction with the value obtained for α,

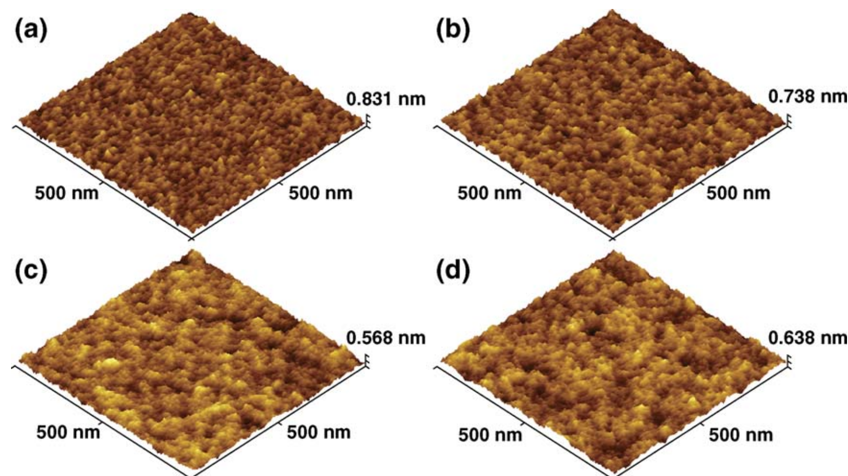

Fig. 2. (Color online) Surface topography of ta-C:H films of different thickness: (a) 1 nm, (b) 13 nm, (c) 52 nm and (d) 110 nm. x- and y-axis are 500 nm in length, while the length of the z-axis is as shown.

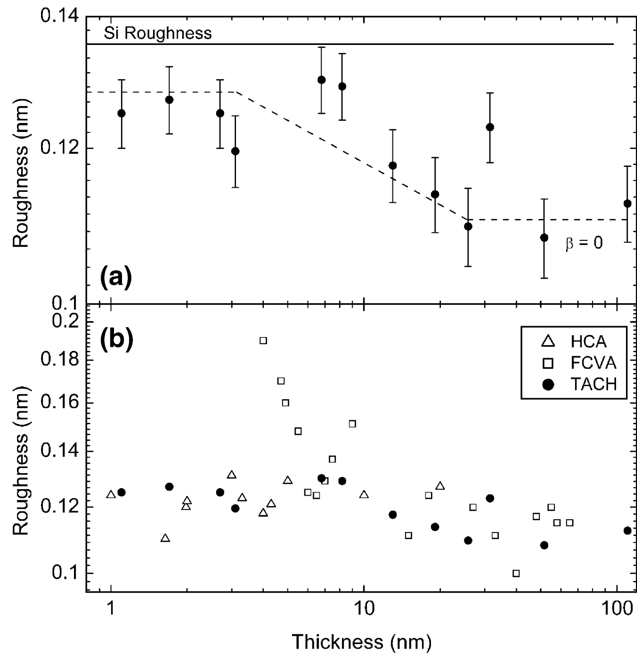

Fig. 3. (a) Variation of the surface roughness versus film thickness. The dashed line is to guide the eye. The continuous line indicates the measured roughness of the bare crystalline silicon substrate. Films thinner than ~10 nm are affected by the underlying rougher substrate. The thicker films have a roughly constant roughness, therefore $\beta=0$. (b) Comparison of the roughness measured for ta-C:H and the data for ta-C from Ref. [14].

we get $\beta=0.09\pm0.03$, in good agreement with Fig. 3. The values for α and β obtained here are very similar to the values previously obtained for ta-C under the same assumption of $\alpha\neq0$ (0.39 and 0–0.1, respectively) [14].

We have recently shown that the smoothening process observed in ta-C is due to impact-induced downhill currents by the energetic ions, and therefore the scaling of the surface of ta-C follows the Edward-Wilkinson model [15,27]. This in turn indicates that the experimental determination of α is better performed using frequency analysis.

Fig. 6a shows the power spectral density function for a 26-nm thick film, indicating the linear region where the Fourier index was determined. We find average Fourier index $i=2.23\pm0.2$. Since $i=2(\alpha+1)$, this is consistent with $\alpha\approx0$, which,

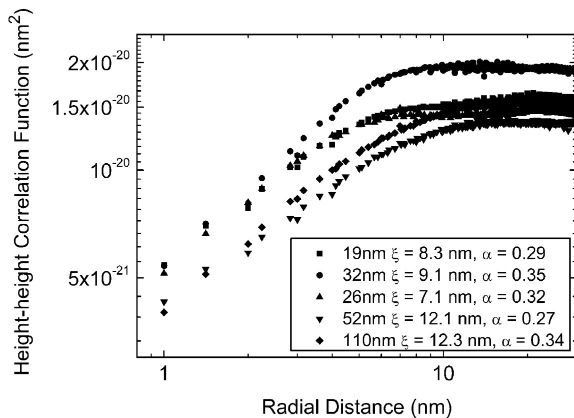

Fig. 4. Height–height correlation function of ta-C:H films for different thickness, indicating the extracted correlation length ξ and roughness exponent α.

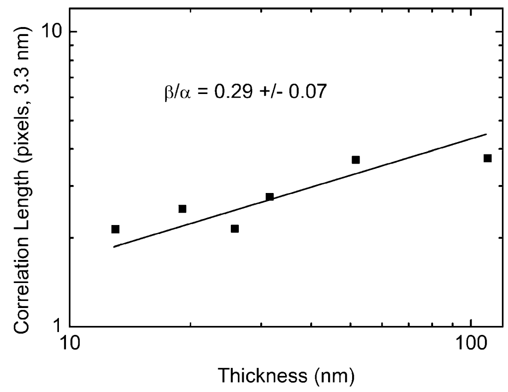

Fig. 5. Correlation length versus film thickness. The slope of the linear fit gives the ratio β/α.

combined with the previously determined $\beta\approx0$, confirms that, similarly to ta-C, the surface evolution of ta-C:H can be well described by the Edwards-Wilkinson theory.

Within the ion-induced downhill currents smoothing mechanism proposed for ta-C, the PSD of the Edwards-Wilkinson equation can be derived analytically as [15,33]:

$$\langle|h(|\mathbf{k}|,t)|^2\rangle = \exp(-2\nu k^2 t)\langle|h(|\mathbf{k}|,0)|^2\rangle + \Omega\frac{1-\exp(-2\nu k^2 t)}{2\nu L^2 k^2}, \quad (11)$$

where L is the lateral size of the system, $\nu=c_2$ is the downhill current strength, and Ω is the volume of a growth unit (atom,

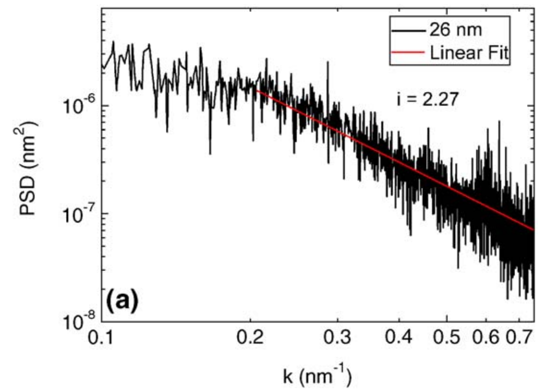

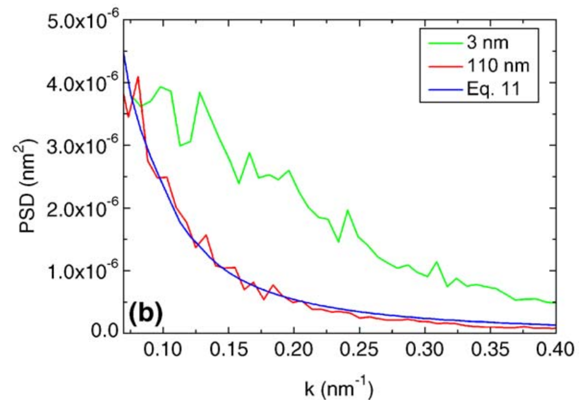

Fig. 6. (Color online) (a) PSD of the 26 nm thick film (black) and the linear fit (red), giving a Fourier index $i=2.27$. (b) PSD of the 110 nm (red) and 3 nm (green) films and a plot of Eq. (11) (blue).

molecule, or cluster) [35]. Molecular dynamics simulations of the growing ta-C:H surface should be performed to derive ν and Ω. However, here we estimated them from Ref. [15], by extrapolating the ta-C results. Fig. 6b compares the predicted PSD evolution for a 110-nm thick film with the PSD directly derived from experiments. Here we used the 3-nm thick film as input for $h(\mathbf{k},0)$. We also assumed $\nu = 1$ nm (for a 170 eV $C_2H_2^+$ ion with 78 eV per carbon atom) [15] and $\Omega = 0.03$ nm^3 [35]. The excellent agreement of the predicted trend with the measured one confirms the general applicability of the smoothening mechanism described in Ref. [15].

5. Conclusions

The surface roughness evolution for ta-C:H was extensively analysed. We determined the growth exponents α and β and found a very similar behaviour to ta-C, with the ta-C:H roughness slightly higher than the ta-C one for any given thickness. The smoothening was assigned to impact-induced downhill currents during growth [15]. This indicates that ta-C:H, similarly to ta-C, benefits from the energetic ion bombardment during deposition that produces extremely smooth films.

Acknowledgement

The authors thank M. Moseler for useful discussions. Funding from the European Community (FAMOUS; Project IST-2000-28661) is acknowledged. A. C. F. acknowledges funding from The Royal Society.

References

[1] J. Robertson, Mater. Sci. Eng., R Rep. 37 (2002) 129.
[2] A.C. Ferrari, J. Robertson, Phys. Rev., B 61 (2000) 14095.
[3] C. Casiraghi, A.C. Ferrari, J. Robertson, Phys. Rev., B 72 (2005) 085401.
[4] A.C. Ferrari, A. Libassi, B.K. Tanner, V. Stolojan, J. Yuan, L.M. Brown, S.E. Rodil, B. Kleinsorge, J. Robertson, Phys. Rev., B 62 (2000) 11089.
[5] A.C. Ferrari, J. Robertson, M.G. Beghi, C.E. Bottani, R. Ferulano, R. Pastorelli, Appl. Phys. Lett. 75 (1999) 1893.
[6] N.A. Morrison, S.E. Rodil, A.C. Ferrari, J. Robertson, W.I. Milne, Thin Solid Films 337 (1999) 71.
[7] M. Weiler, K. Lang, E. Li, J. Robertson, Appl. Phys. Lett. (1998) 1314.
[8] N.A. Morrison, S. Muhl, S.E. Rodil, A.C. Ferrari, M. Nesladek, W.I. Milne, J. Robertson, Phys. Status Solidi, A Appl. Res. 172 (1999) 79.
[9] M. Weiler, S. Sattel, T. Giessen, K. Jung, H. Ehrhardt, V.S. Veerasamy, J. Robertson, Phys. Rev., B 53 (1996) 1594.
[10] M. Weiler, S. Sattel, K. Jung, H. Ehrhardt, V.S. Veerasamy, J. Robertson, Appl. Phys. Lett. 64 (1994) 2797.
[11] B. Kleinsorge, S.E. Rodil, G. Adamopoulous, J. Robertson, D. Grambole, W. Fukarek, Diamond Relat. Mater. 10 (2001) 965.
[12] H.H. Gatzen, M. Beck, Tribol. Int. 36 (2003) 279.
[13] A.C. Ferrari, Surf. Coat. Technol. 180–181 (2004) 190.
[14] C. Casiraghi, A.C. Ferrari, R. Ohr, A.J. Flewitt, D.P. Chu, J. Robertson, Phys. Rev. Lett. 91 (2003) 226104.
[15] M. Moseler, P. Gumbsch, C. Casiraghi, A.C. Ferrari, J. Robertson, Science 309 (2005) 1545.
[16] F. Piazza, D. Grambole, L. Zhou, F. Talke, C. Casiraghi, A.C. Ferrari, J. Robertson, Diamond Relat. Mater. 13 (2004) 1505.
[17] C. Casiraghi, A.C. Ferrari, J. Robertson, Diamond Relat. Mater. 14 (2005) 913.
[18] J. Robertson, Tribol. Int. 36 (2003) 405.
[19] P.R. Goglia, J. Berkowitz, J. Hoehn, A. Xidis, L. Stover, Diamond Relat. Mater. 10 (2001) 271.
[20] C. Casiraghi, A.C. Ferrari, J. Robertson, R. Ohr, M.v. Gradowski, D. Schneider, H. Hilgers, Diamond Relat. Mater. 13 (2004) 1480.
[21] T. Schulke, A. Andres, P. Siemroth, IEEE Trans. Plasma Sci. 25 (1997) 660.
[22] K.B.K. Teo, S.E. Rodil, J.T.H. Tsai, A.C. Ferrari, J. Robertson, W.I. Milne, J. Appl. Phys. 89 (2001) 3706.
[23] R. Ohr, B. Jacoby, M.v. Gradowski, C. Schug, H. Hilgers, Surf. Coat. Technol. 174–175 (2003) 1135.
[24] X.L. Peng, Z.H. Barber, T.W. Clyne, Surf. Coat. Technol. 138 (2001) 23.
[25] S. Sattel, J. Robertson, H. Ehrhardt, J. Appl. Phys. 82 (1997) 4566.
[26] C. Casiraghi, A.C. Ferrari, R. Ohr, D. Chu, J. Robertson, Diamond Relat. Mater. 13 (2004) 1416.
[27] A.-L. Barabasi, H.E. Stanley, Fractal Concepts in Surface Growth, Cambridge University Press, Cambridge, 1995.
[28] F. Family, T. Vicsek, J. Phys., A, Math. Gen. 18 (1985) L75.
[29] S. Edwards, D. Wilkinson, Proc. R. Soc. Lond., A 44 (1966) 1039.
[30] M. Kardar, G. Parisi, Y. Zhang, Phys. Rev. Lett. 56 (1986) 889.
[31] A.H.M. Smets, W.M.M. Kessels, M.C.M.v.d. Sanden, Appl. Phys. Lett. 82 (2003) 865.
[32] K.R. Bray, G.N. Parsons, Phys. Rev., B 65 (2002) 035311.
[33] W.M. Tong, R.S. Williams, Annu. Rev. Phys. Chem. 45 (1994) 401.
[34] S.K. Sinha, E.B. Sirota, S. Garoff, H.B. Stanley, Phys. Rev., B 38 (1988) 2297.
[35] D.G. Stearns, Appl. Phys. Lett. 62 (1993) 1745.